



Verification and validation of Reynolds-averaged Navier–Stokes turbulence models for external flow [☆]



Jacob A. Freeman ^{a,*}, Christopher J. Roy ^b

^a United States Air Force, United States

^b Department of Aerospace & Ocean Engineering, Virginia Tech, 215 Randolph Hall, Blacksburg, VA 24061, USA

ARTICLE INFO

Article history:

Received 26 June 2013

Received in revised form 1 November 2013

Accepted 5 November 2013

Available online 27 November 2013

Keywords:

Verification and validation

Code verification

Solution verification

Reynold-averaged Navier–Stokes turbulence models

Subsonic compressible flow

Computational fluid dynamics

ABSTRACT

The Spalart–Allmaras (S-A) turbulence model in the NASA–Langley CFL3D and FUN3D flow solvers has been previously verified 2nd-order accurate. For low subsonic 2-D applications (turbulent flat plate and NACA 0012 airfoil at $\alpha = 0^\circ$), solutions from the S-A, S-A with Rotation and Curvature (SARC), Menter Shear-Stress Transport (SST), and Wilcox 1998 $k-\omega$ turbulence models in commercial flow solvers, Cobalt and RavenCFD, are compared with NASA results for code verification. Of 36 case evaluations, each of which uses 5 systematically refined computational meshes, only 7 approach 2nd-order observed accuracy, but 27 cases show 1st-order or better, indicating the formal order may be less than 2 for these applications. Since Cobalt and RavenCFD turbulence models perform comparable to NASA's verified models and since rigorous code verification is not possible without access to source code, the presented evidence suggests these turbulence models are implemented correctly for these or similar flow conditions and configurations. For solution verification, estimates of numerical uncertainty are less than 0.5% for 94% of the cases and less than 0.1% for 61% of the cases. For validation, the turbulent flat plate solutions match experiment skin friction within 4.8% for $x/L > 0.05$, and for airfoil drag coefficient, S-A and SST agree within 1.2% of experiment, SARC 2%, and $k-\omega$ 4%.

Published by Elsevier Masson SAS.

1. Introduction

With initial and subsequent versions of flow solvers, developers and users subject the code to a suite of regression tests and case validations, such as the 1-D Riemann shock-tube problem [14]; in 2-D, an inviscid supersonic inlet with compression ramp [14], inviscid airfoil in transonic flow, inviscid base flow [10], laminar flat plate [14], viscous, turbulent boundary-layer flow for the flat plate, supersonic ramp, and an airfoil [3,4,6,10–12,15,16,21,24,30], or various types of jet and shear flow [1,2]; then well tested 3-D applications such as a supersonic missile with fins [14], a wing [11,30], or a civil air transport in transonic cruise [29]. Often, however, little attention is given to code verification (to determine the code's observed order of accuracy, as compared with its formal order) or to solution verification (to quantify numerical accuracy of the code's predicted solutions) [18]. The preference is to verify a code's formal order of accuracy by computing the solution to a problem with an exact solution. The exact analytical solution or an

exact manufactured solution may then be used to accomplish this code verification [18]. Without access to source code, in the case of commercial flow solvers, the user may conduct code verification by carefully comparing results with those from a flow solver that has been rigorously verified. To conduct solution verification, users may then use the verified code to compute solutions for various applications and estimate the numerical error in those solutions, effectively placing “error bars” on the computational predictions. As the last step in the verification and validation process, the user validates the model to assess how accurately the model represents the physical flow; this is accomplished by comparing the computed solution with experimentally obtained data.

The purpose of this study is to verify turbulence models in the commercial flow solvers, Cobalt and RavenCFD, which are derived separately from the Air Force Research Lab's *Cobalt*₆₀, by comparing their solutions and behavior with those obtained from the previously verified NASA–Langley flow solvers, CFL3D (cell-centered structured) and FUN3D (node-centered unstructured) [20,22]. The code and solution verification are performed using two subsonic, 2-D turbulent applications: flat plate and NACA 0012 airfoil at angle of attack, $\alpha = 0^\circ$. These applications were selected because their combined features may represent a more complex, 3-D subsonic flow field. These verification activities compare results from four Reynolds-averaged Navier–Stokes (RANS) turbulence models: Spalart–Allmaras (S-A), S-A with corrections for

[☆] The views expressed in this article are those of the authors and do not necessarily reflect the official policy or position of the U.S. Air Force, the U.S. Department of Defense, or the U.S. Government.

* Corresponding author. Tel.: +1 3106534117.

E-mail addresses: jacob.freeman@us.af.mil (J.A. Freeman), cjroy@vt.edu (C.J. Roy).

¹ Lieutenant Colonel.

rotation and curvature (SARC), Wilcox 1998 $k-\omega$, and Menter shear-stress transport (SST). Model validation is not stressed in this study, but there is some validation for each case. While the flow solvers, turbulence models, and test cases are specific to this study, the *process* by which code and solution verification are conducted for commercial code may be broadly applied throughout the computational community.

2. Background and methods

2.1. Flow solvers

Cobalt [7] solves the 3-D unsteady, compressible Euler and Navier–Stokes equations at cell centers, uses the method of finite volumes, and is parallelized. It is designed to use structured or unstructured mesh topologies, including prisms, tetrahedra, and hexahedra in 3-D, or quadrilaterals and triangles in 2-D, all with arbitrary cell skewness, curvature and/or stretching rates. Cobalt combines the exact Riemann solver of Gottlieb and Groth [13] and the approximate Riemann solver of Harten–Lax–van Leer–Contact (HLLC) [26] with a least-squares method to attain 2nd-order spatial accuracy, and it uses a point-implicit method with Newton sub-iterations for 2nd-order temporal accuracy. Its implicit method allows for Courant–Friedrichs–Lewy (CFL) numbers as large as 1×10^6 . Cobalt offers eight turbulence models, including the four used for this study, which have formally 2nd-order accurate numerical implementations but may revert to 1st-order in the presence of discontinuities, contact surfaces, large flow gradients, or singularities. Cobalt offers one discontinuous flux limiter which may influence the solution observed order of accuracy [7,14,29].

RavenCFD [8] also solves the 3-D unsteady, compressible Euler and Navier–Stokes equations at cell centers, uses finite volumes, is parallelized, may use structured or unstructured mesh topologies, is formally 2nd-order accurate in space and time, uses Newton sub-iterations with its implicit solver, and allows the following options to users: fully implicit or explicit using a 4-stage Runge–Kutta solver; flux-splitting schemes of either Gottlieb and Groth [13] or Edwards Low-Diffusion (LDFSS) [27], which is designed primarily for reacting and multi-phase flows; local or global time-stepping; wall functions; and various flux limiters [5]. All RavenCFD simulations in this study use the minmod limiter. RavenCFD offers nine turbulence models, including three used for this study, all with 2nd-order numerical implementations that may reduce to 1st-order when exposed to the effects noted above. RavenCFD does not include the SARC turbulence model.

2.2. Turbulence models

To reduce computational mesh cell count and overall computation time for applications with large Reynolds number flow, all scales of turbulent flow are modeled with RANS turbulence models in this study. The turbulence models include the S-A one-equation (meaning one transport partial differential equation), SARC one-equation, Wilcox 1998 $k-\omega$ two-equation, and Menter SST two-equation. For the detailed equations and coefficients used by these turbulence models, see [10,20,25]. Care is taken to ensure turbulence model equations and coefficients are common among all flow solvers in this study, including one revision to a RavenCFD SST coefficient for conformity.

The S-A turbulence model is often applied to aircraft applications, including predicting separation due to adverse pressure gradients. The S-A model is a function of velocity, kinematic viscosity, vorticity, and wall distance. In the laminar sub-layer it uses a wall-destruction function to reduce turbulent viscosity, and to transition the boundary layer from laminar to turbulent it includes

trip functions. The S-A model relies on 11 empirical constants [10]. The SARC model includes a modification in the production term which is a function of kinematic strain and rotation rates, as well as three additional constants [25]. The S-A and SARC models show good agreement with experiment for subsonic flow over a flat plate, sub- and transonic flow over airfoils and wings, rotating and curved channels, and turbulent shear flow [3,4,6,11,12,15,21,24,30].

Wilcox's 1998 $k-\omega$ turbulence model is often used for wall-bounded flow, regions of large separation, and terms were added to better model planar shear layers. The two transport variables are turbulent kinetic energy, k , and turbulent specific dissipation rate, ω , and the model is a function of velocity, kinematic viscosity, and turbulent shear stress. The model includes low Reynolds number corrections for transition from laminar to turbulent boundary layer. The $k-\omega$ model also relies on 11 empirical constants [10]. The $k-\omega$ model shows good agreement with experiment, though generally not as good as the S-A, SARC, and SST models, for subsonic flow over a flat plate and an airfoil, and turbulent shear flow [2,4,6].

Menter's SST turbulence model combines the accuracy of the $k-\omega$ model for wall-bounded flow with that of the $k-\varepsilon$ model for shear flow; the 2nd transport variable is turbulence dissipation, ε . Away from the wall, the ε -equation is transformed into an ω -equation, and the model relies on a computationally expensive switching function between the two sub-models. The SST model is a function of velocity, kinematic viscosity, turbulent shear stress, vorticity, and distance from the wall, and it relies on 10 empirical constants [10]. The SST model shows good agreement with experiment for subsonic flow over a flat plate and sub- and transonic flow over airfoils [3,4,6,11,21]. For the comparisons in this study, Cobalt and RavenCFD use the version of SST discussed above, while FUN3D and CFL3D both use (for the flat plate case, not for the airfoil) a variant form of the SST model, noted SST-V. To improve numerical stability, the SST-V model transport equations include a modification to the vorticity source term [20].

2.3. Case descriptions

The unit tests include a 2-D flat plate to verify and validate boundary layer modeling and a 2-D airfoil for adverse or non-zero pressure gradient modeling.

Fig. 1 shows the 2-D flat plate formulation from NASA-Langley [20], which includes five levels of systematically refined structured meshes; Fig. 1(b) shows the 2nd coarsest of those grids, the finest being 545×385 . Values for the average y^+ for the first cell along the surface range between 0.68 for the coarsest grid to 0.04 for the finest; y^+ is defined as

$$y^+ = \frac{y}{\nu} \sqrt{\frac{\tau_w}{\rho}} = y Re_{/x} \sqrt{\frac{C_f}{2}} \quad (1)$$

where y for this case is the height of the first cell (m), ν is kinematic viscosity (m^2/s), τ_w is wall shear stress (N/m^2), ρ is density (kg/m^3), $Re_{/x}$ is Reynolds number per length (m^{-1}), and C_f is skin friction coefficient. Freestream Mach, $M_\infty = 0.2$, is selected to ensure essentially incompressible flow, though the flow solvers all use compressible equations. Reynolds number is $Re_{/x} = 5 \times 10^6 \text{ m}^{-1}$. Specified at the inflow boundary are total pressure, $P_0 = 117,684.90 \text{ Pa}$, and total temperature, $T_0 = 302.4 \text{ K}$; they are based on specified $T_{ref} = 300 \text{ K}$ and calculated $P_{ref} = 114,448.3 \text{ Pa}$ (from given M_∞ and $Re_{/x}$). At the outflow boundary, $P = P_{ref}$. The plate has no thickness, length is $L = 2.0 \text{ m}$, and skin friction coefficient values are extracted at $x = 0.97008 \text{ m}$, or $x/L = 0.48504$. A point singularity at the plate leading edge poses a potential problem with the setup; the singularity makes it difficult, particularly for node-centered codes, for observed order of accuracy to

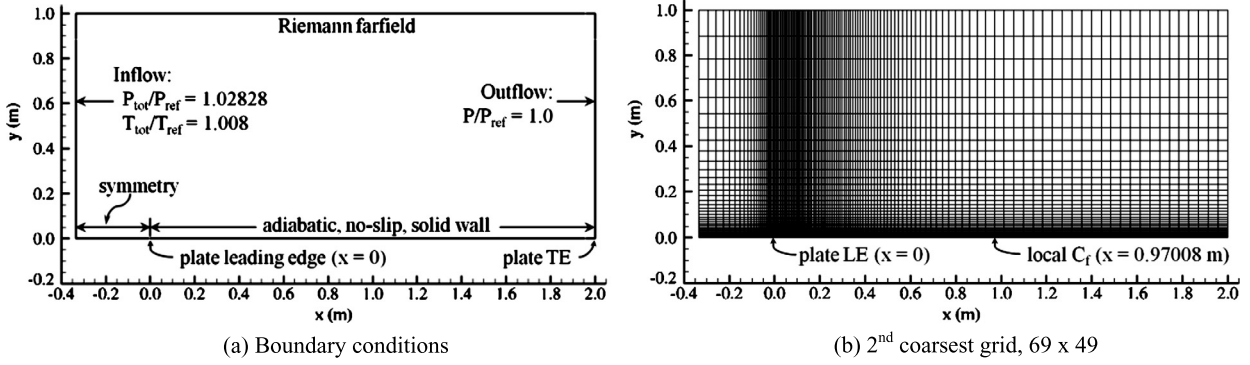


Fig. 1. Turbulent flat plate case, $M_\infty = 0.2$, $Re_L = 1 \times 10^7$ ($L = 2$ m), $T_{ref} = 300$ K.

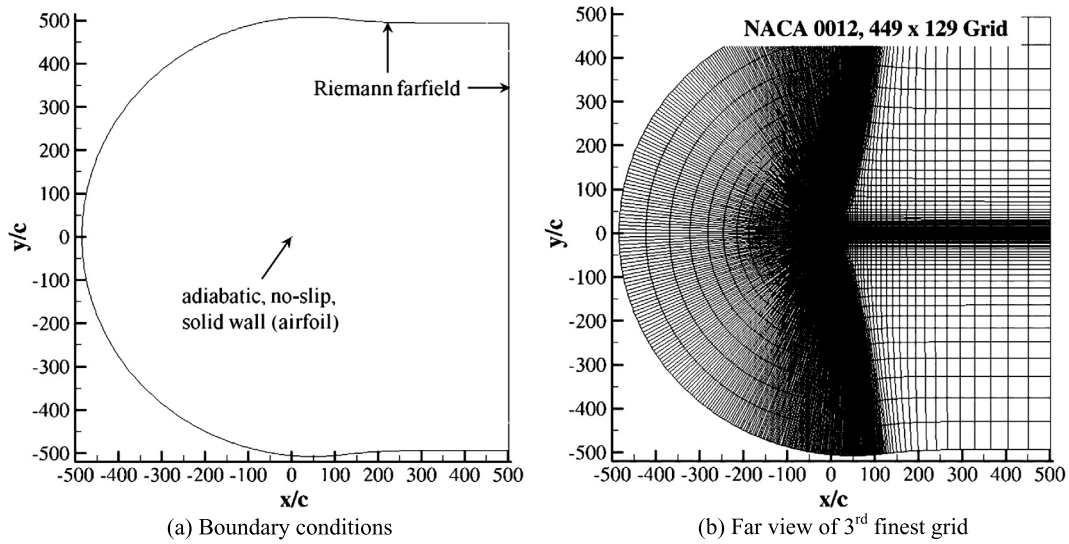


Fig. 2. NACA 0012 airfoil case, $M_\infty = 0.15$, $Re_c = 6 \times 10^6$ ($c = 1$ m), $T_{ref} = 300$ K.

match the formal order [20]. From the flow solvers, skin friction (C_f) and drag (C_d) coefficients are calculated as

$$C_f = \frac{2\tau_w}{\rho u^2} \quad \text{and} \quad C_d = \frac{2F_{x,avg}}{\gamma P_{ref} M_\infty^2 L} \quad (2)$$

where u is local velocity magnitude (m/s), γ is ratio of specific heats (for air, $\gamma = 1.4$), and $F_{x,avg}$ is average force in the axial direction (N).

Fig. 2 shows the NACA 0012 airfoil setup from NASA-Langley [20], which includes five levels of systematically refined curvilinear structured meshes; Figs. 2(b) and 2(c) show the 3rd finest of those grids, the finest being 1793×513 or 917,504 cells. The computational domain extends 500 chord lengths in all directions to fully capture circulation effects. Values for the average y^+ for the first cell along the surface range between 1.19 for the coarsest grid to 0.048 for the finest. Freestream Mach, $M_\infty = 0.15$, is selected to ensure essentially incompressible flow, and Reynolds number

per chord length is $Re/c = 6 \times 10^6/c$, where $c = 1.0$ m. At the Riemann farfield boundary, $T_{ref} = 300$ K and $P_{ref} = 183,117.4$ Pa. Because the primary interest is code verification using this model, only the $\alpha = 0^\circ$ case is evaluated and only C_d and C_f are considered, since $C_l = 0$ at this angle for a symmetric airfoil. C_f is evaluated locally at a point on the upper surface ($x/c = 0.5121166$, $y/c = 0.0513979503$). For the single validation point, C_d at $\alpha = 0^\circ$, comparison is made with Ladson's experimental results [17] because the boundary layer is tripped and thus fully turbulent. From the flow solvers, C_d and C_f are calculated as in Eq. (2), since $\alpha = 0^\circ$ and for $L = c$. This case differs from the flat plate case by incorporating a non-zero pressure gradient on the surfaces, by removing the leading edge singularity, and by changing the boundary conditions from inflow/outflow to farfield.

2.4. Code verification

Two primary intents of code verification include (1) ensuring a code is correct and bug-free, and (2) proving that systematic mesh refinement results in improved observed order of accuracy, i.e., as the cell spacing approaches zero, the observed order of accuracy should approach the formal order of accuracy [18,19]. Since the commercial codes being evaluated are well tested and free of blatant errors, the second intent is addressed in this study. To accomplish this, multiple, systematically refined mesh levels are used; systematic refinement requires uniformity (constant refinement factor in all spatial directions) and consistency (as cell size approaches zero, the mesh quality – cell aspect ratio, stretching factor, skewness and curvature – remains the same or improves) [18]. For all three cases, NASA-Langley [20] generated a fine grid, removed every other grid point in each spatial direction for the next coarser grid, and repeated until five grid levels were created. From the flow solvers' integrated values for C_d , for example, the observed order of accuracy [18] is calculated as

$$\hat{p} = \frac{\ln \left| \frac{C_{d,3} - C_{d,2}}{C_{d,2} - C_{d,1}} \right|}{\ln(r)} \quad (3)$$

where the indices 1, 2, and 3 denote solutions from systematically coarser grids, respectively, 1 being the solution from the finest of the three grids; and r is grid refinement factor, or $r = \left(\frac{N_{cells,1}}{N_{cells,2}} \right)^{1/2} = 2$ for all of these grids. Thus, if the observed order of accuracy approaches the formal order within an acceptable margin (e.g., 10%), or if the observed order behaves similarly to that of a verified code, the code of interest may not be declared unequivocally verified but the model is probably implemented correctly.

2.5. Solution verification

To verify the solution, numerical error must be quantified, where numerical error consists of error due to round-off, iterations, discretization, and statistical sampling. Numerical uncertainty can be quantified by applying a factor of safety to the absolute value of the numerical error [19]. The cases examined do not result in any statistical sampling error, but using double-precision computations in the flow solvers generally keeps round-off error to much less than 1% of the discretization error. Iterative error is the difference between the current iterative approximate solution and the exact solution to the discrete equations, and the "machine-zero method" is used to estimate this error. With the machine-zero method, the solution residuals are iteratively converged either to machine zero (14 orders of magnitude for double-precision) or as far as the solver permits with its stabilizing functions (flux limiters and damping), then that deeply converged solution is compared with the solution at the current iterative level to estimate the iterative error [18,19]. For the cases in this study, iterative error

estimates are assumed to be zero because every solution is converged as far as the schemes allow, between 6 and 10 orders of magnitude reduction in the iterative residual for the continuity equation.

Before estimating the discretization error and uncertainty in the numerical error, the exact solution is first approximated via Richardson Extrapolation [19]. Richardson Extrapolation generally provides an estimate that is one order more accurate than the computed results; e.g., if using a formally 2nd-order method, Richardson Extrapolation estimates a solution that is 3rd-order accurate, and it requires solutions from the two finest systematically refined grids. Again using C_d as an example, the extrapolated value $\bar{C}_{d,RE}$ is calculated as

$$\bar{C}_{d,RE} = C_{d,1} + \frac{(C_{d,1} - C_{d,2})}{r^{\hat{p}} - 1} \quad (4)$$

We then use the extrapolated value to estimate the discretization error,

$$\bar{\epsilon}_{DE,RE} = |C_{d,i} - \bar{C}_{d,RE}| \quad (5)$$

where i is the respective grid level.

Lastly the uncertainty due to numerical error is approximated according to the sum of its parts, $U_{Numerical} = U_{Discretization Error} + U_{Iterative Error} + U_{Round-off Error}$, where $U_{Iterative Error} = |C_{d,iter level} - C_{d,machine zero}| = 0$ for these cases, $U_{Round-off Error} \approx 0.01(\bar{\epsilon}_{DE,RE})$, and using Roache's Grid Convergence Index with a modified implementation by Oberkampf and Roy [19] for the factor of safety, F_s , when using solutions on three or more systematically refined meshes,

$$U_{Discretization Error} = \frac{F_s}{r^{\hat{p}} - 1} |C_{d,i} - C_{d,i+1}| \quad \text{where} \quad (6)$$

$$F_s = 1.25 \quad \text{for } \chi = \left| \frac{\hat{p} - p_f}{p_f} \right| \leq 0.1, \quad \text{or } F_s = 3 \quad \text{for } \chi > 0.1$$

and where i is the grid refinement level, p_f is formal order of accuracy, and \hat{p} is defined in Eq. (3). To avoid double penalizing the discretization error estimate, $p = \hat{p}$ if $F_s = 1.25$, and $p = p_f$ if $F_s = 3$.

3. Results and discussion

3.1. 2-D turbulent flat plate

For code verification, Figs. 3(a) and 3(b) show the turbulent flat plate's predicted drag coefficients from the four flow solvers using two to four RANS turbulence models on five systematically refined meshes. (Note: There are no data for FUN3D and CFL3D using $k-\omega$, and SARC results are available only for Cobalt.) Figs. 3(c) and 3(d) show predicted skin friction coefficient at $x/L = 0.48504$. Dashed-black lines mark $\pm 1\%$ of the average C_d or C_f from the NASA solutions, or benchmark numerical solution. The grid refinement parameter, h , is defined spatially [15] as

$$h = \Delta x / \Delta x_{ref} \quad (7)$$

where Δx_{ref} refers to the finest grid spatial node spacing; e.g., $h = 1$ corresponds to the finest grid. Cobalt and RavenCFD S-A solutions coincide for both C_d and C_f within 0.01% or less; thus, they appear as one line in each plot. On the finest grid for the S-A model, each of the four codes predicts a value for C_d and C_f within 0.3% of the others. Cobalt SARC results also nearly coincide with Cobalt S-A results (less than 0.2% for C_d and C_f for all grid levels); the small difference between S-A and SARC is unsurprising because neither curvature nor significant rotation is present. On the finest grid for the SST model, each of the four codes predicts

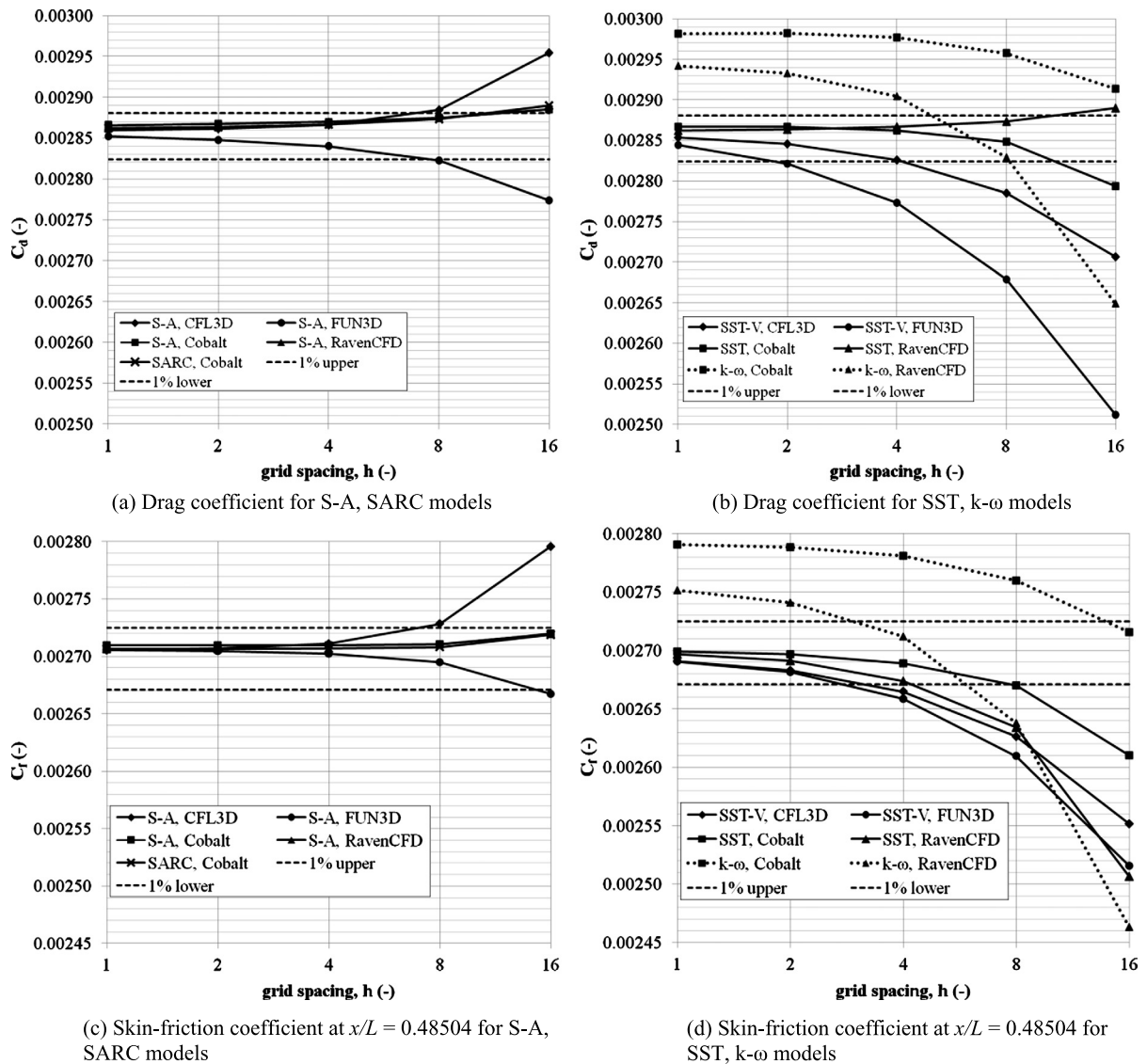


Fig. 3. Turbulent flat plate using RANS turbulence models on 5 systematically refined meshes, $M_\infty = 0.2$, $Re_L = 1 \times 10^7$ ($L = 2$ m), $T_{ref} = 300$ K.

a value for C_d and C_f within 0.5% of the others; although small, most of that gap comes from the difference between the SST and SST-V models. On the finest grid for the $k-\omega$ model in Cobalt and RavenCFD, however, differences range between 2.0 and 4.5% from the NASA average for the S-A and SST models; this larger difference occurs in part because the $k-\omega$ model creates greater eddy viscosity within the boundary layer, as shown in more detail in Fig. 4. Further, since Cobalt and RavenCFD $k-\omega$ results on the finest grid differ from each other by 1.4% for both C_d and C_f , there must be a slight difference in their implementation and/or an effect of flux limiter switching (in Cobalt) that is most likely.

In Fig. 4, ratios of turbulent eddy viscosity to freestream viscosity (μ_t/μ_∞) are compared for the various RANS turbulence models. Figs. 4(a) and 4(b) show contours of the difference between the $k-\omega$, S-A, and SST models, indicating clearly larger values for eddy viscosity within the flat plate boundary layer generated by the $k-\omega$ turbulence model; for reference, the dashed line shows the $k-\omega$ boundary layer thickness, noted as $\delta_{0.99}$ and based on where the local velocity (in the x -direction) magnitude is 99% of the freestream velocity. Fig. 4(c) further illustrates that the $k-\omega$ model generates the most turbulent eddy viscosity within the boundary layer, and it strengthens the argument that the commercial flow solvers' turbulence models are implemented correctly for the tur-

bulent flat plate case, since the results and behavior match so closely with the benchmark codes. Specifically at streamwise location, $x/L = 0.48504$, the eddy viscosity ratio for Cobalt's S-A model differs from that of FUN3D by less than 1.7% with respect to the maximum value ($<0.1\%$ for 3/4 of the shear layer), and Cobalt SST differs from FUN3D SST-V by less than 4.3% ($<0.2\%$ for 3/4 of the shear layer); Cobalt S-A and SARC differ by less than 1.6% throughout the shear layer, and Cobalt S-A and $k-\omega$ differ by as much as 39%. While not plotted in Fig. 4(c), RavenCFD turbulence models predict an eddy viscosity ratio at that location that differs from the Cobalt results by less than 0.02% for S-A, 0.8% for SST, and 8% for $k-\omega$.

Figs. 5(a) and 5(b) show the local value for C_f along the flat plate surface from each of the turbulence models, as well as an empirically-based integral solution, noted "MOSES, fully turbulent," and experimental results from Wieghardt and Tillmann [28], which are discussed later. The integral method [23] uses Moses' turbulent mean-flow momentum integral equations, neglects the effects of a transition region, is based on empirical data to model the turbulent eddy viscosity, approximates the wake function to provide a more representative boundary layer velocity profile, assumes steady (in the mean) turbulent flow, and treats all dependent variables as mean values. The associated solvers [9] assume incompressible

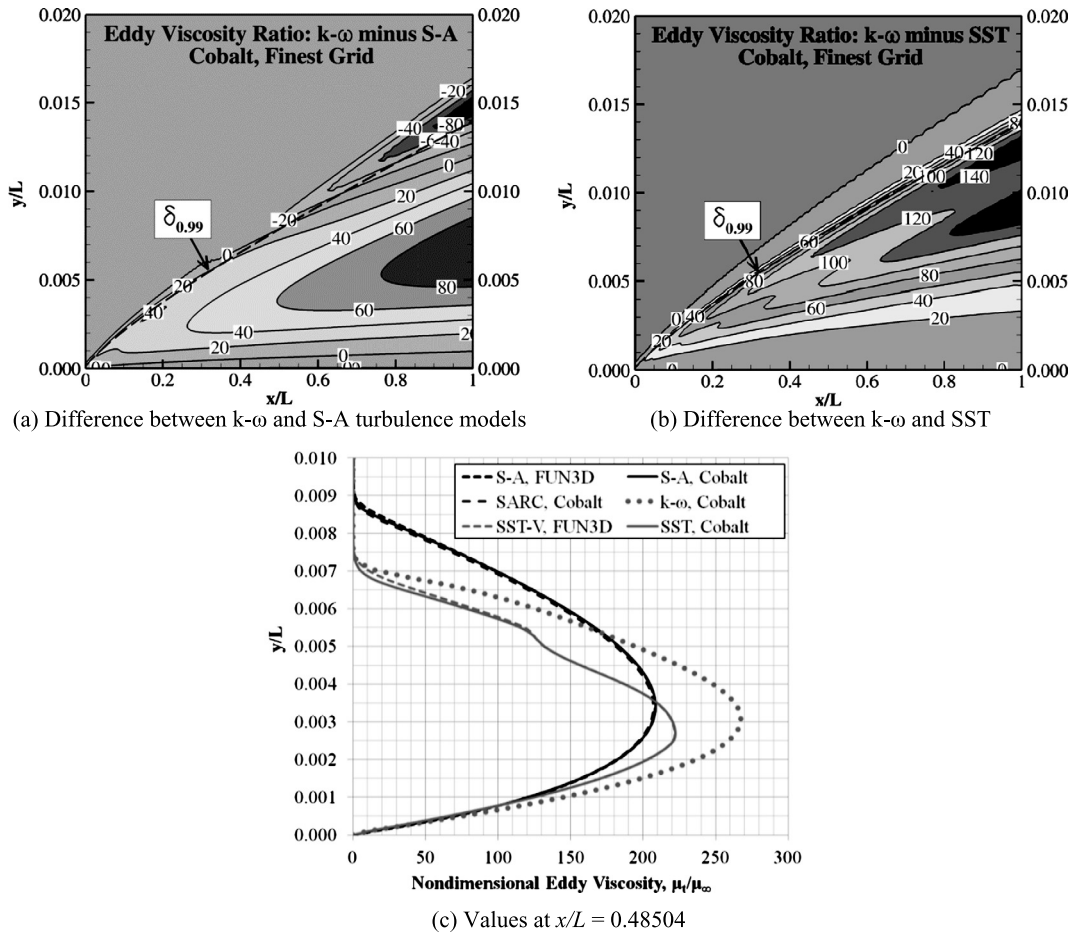


Fig. 4. Turbulent eddy viscosity ratios (μ_t/μ_∞) normal to flat plate surface, finest grid, $M_\infty = 0.2$, $Re_L = 1 \times 10^7$ ($L = 2$ m), $T_{ref} = 300$ K.

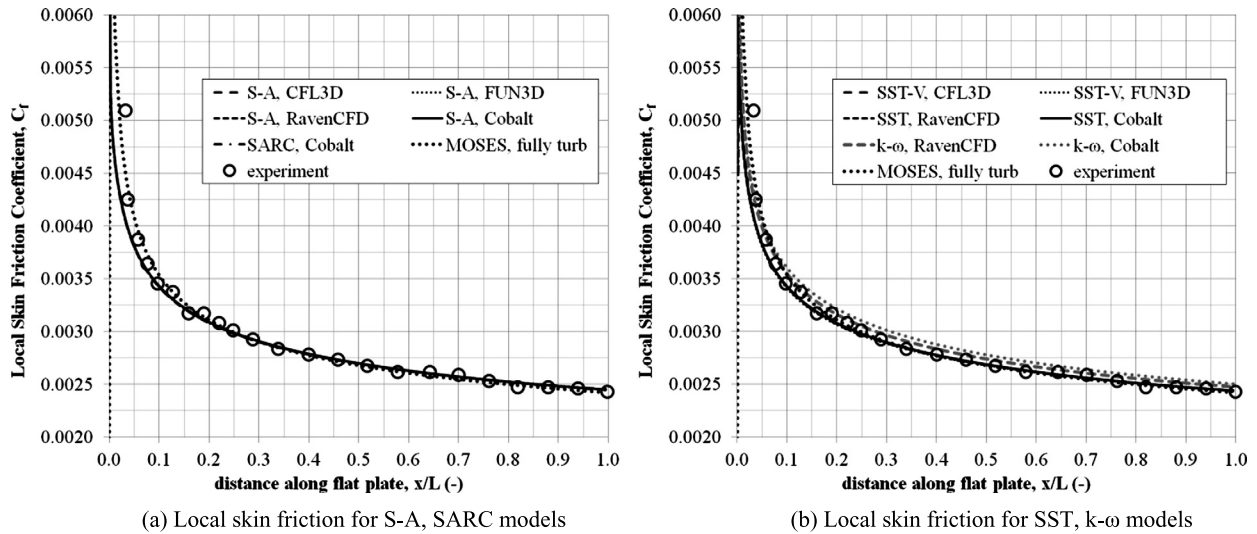


Fig. 5. Skin friction coefficient along flat plate surface from solutions on finest grid (545×385), $M_\infty = 0.2$, $Re_L = 1 \times 10^7$ ($L = 2$ m), $T_{ref} = 300$ K.

flow but allow a viscous calculation for the surface flow. As noted in [20], agreement suffers at the leading and trailing edges because of the point singularities; however, along the rest of the surface the S-A, SARC, and SST models agree with each other within less than 0.4%, and the $k-\omega$ models differ from each other by 1.1–1.6%.

For code verification, observed order of accuracy for C_d and C_f is shown in Table 1, based on the solutions to the three finest grids (with two noted exceptions), for the several turbulence models and

flow solvers; for solution verification, Table 1 also shows total estimated uncertainty due to numerical error. A negative value for observed order of accuracy means the difference between solutions from grid levels 2 and 3 is smaller than the difference from grid levels 1 and 2. Accuracy for C_f at a point is generally better than or comparable to C_d because the local C_f value is less affected by the leading edge singularity. Observed order of accuracy near unity is noted in several cases, likely due to that singularity

Table 1
Turbulent flat plate observed order of accuracy and total numerical uncertainty.

Turbulent flat plate, $M = 0.2$, $Re_L = 10 \times 10^6$ ($L = 2$ m)					
Turbulence model	Flow solver	C_d		C_f at $x/L = 0.48504$	
		\hat{p}	$U_{Tot,Num}$	\hat{p}	$U_{Tot,Num}$
S-A	CFL3D	1.75	0.03%	1.98	0.02%
	FUN3D	0.80	0.48%	1.34	0.03%
	Cobalt	0.83	0.15%	<0	0.03%
	RavenCFD	1.00	0.06%	<0	0.03%
SST-V	CFL3D	1.34	0.22%	1.21	0.28%
	FUN3D	1.07	0.92%	1.39	0.26%
SST	Cobalt	1.75 ^a	0.08% ^a	1.84	0.04%
	RavenCFD	0.93	0.04%	1.60	0.13%
k- ω	Cobalt	1.87 ^a	0.08% ^a	1.65	0.05%
	RavenCFD	1.63	0.19%	1.50	0.26%
SARC	Cobalt	0.93	0.08%	2.17	0.001%

^a Results taken from coarser level of grids due to oscillatory behavior on finest level.

(C_f approaches infinity at the leading edge). In general, numerical uncertainty is less than 1% for all cases and is smaller for cases where the observed order is close to the formal order of accuracy, which is assumed to be 1.0 for the error and uncertainty calculations for the integrated coefficient, C_d . That is, if $0.9 \leq \hat{p} \leq 2.2$, then $F_s = 1.25$ for Eq. (6) since 1st-order effects are present. It is imprecise to declare that these flow solvers display 2nd-order accuracy for all the turbulence models evaluated, and the results in Table 1 suggest the formal order for this case is likely between 1 and 2. It may be concluded that the results from these Cobalt and RavenCFD RANS turbulence models closely match results from the numerical benchmark codes, CFL3D and FUN3D, which have been verified for the S-A turbulence model [22], and that the turbulence models have been correctly implemented for turbulent boundary layer flow.

For validation, Figs. 5(a) and 5(b) show the local C_f comparison with the experiment of Wieghardt and Tillmann [28]. The computational results for the finest grid do not agree well with experiment at the two measured points closest to the leading edge, $x/L < 0.05$, where the results differ from experiment by 5–20%; this is possibly due to interference from the pressure rake in the boundary layer transition region. At every other measured location, the simulations from all four flow solvers and all turbulence models differ from the experiment by less than 4.0%, with the one exception of Cobalt k- ω , which differs by as much as 4.8%. Again disregarding the two points nearest the leading edge, the average difference between computation and experiment for C_f is 0.9–1.0% for the S-A, SST, and SARC turbulence models; Cobalt and RavenCFD results for k- ω differ on average from experiment by 3.2% and 1.8%, respectively. These results are consistent with other subsonic-flow flat-plate comparisons between computation and experiment for these four turbulence models [3,4,6,15,21]. Thus, it may reasonably be concluded for the turbulent flat plate skin friction that the RANS turbulence models all compare well with experiment for $x/L > 0.05$.

3.2. 2-D NACA 0012 airfoil at $\alpha = 0^\circ$

For the airfoil case, NASA-Langley [20] conducted primarily a validation study so verification data are less complete; specifically, they provide C_d results from CFL3D and FUN3D for only the 2nd finest grid and C_f results from only CFL3D on the 2nd finest grid. However, C_d results on that grid are included from one additional flow solver, from the Russian NTS. Also, CFL3D and FUN3D results include the SST turbulence model without the additional vorticity source term. For code verification, Figs. 6(a) and 6(b) show the NACA 0012 predicted drag coefficients; Figs. 6(c) and 6(d) show the predicted skin friction coefficient at the upper-surface location

noted in Section 2.3. Dashed-black lines mark $\pm 1\%$ of the average C_d or C_f from the NASA benchmark numerical solutions, again for the 2nd finest grid in this case. Some coarse-grid results are truncated from Fig. 6 to accentuate the more pertinent results on the finer grids. For C_d predictions on the finest grid, the SST solutions from Cobalt and RavenCFD differ from each other by 0.03%. S-A results for C_d predictions on the finest grid differ from each other by 0.08%, and SARC results differ from S-A by 2.6% showing that this turbulence model slightly under-predicts the eddy viscosity. (Refer to Fig. 4(c), where SARC predicts boundary-layer eddy viscosity ratios 1.6% less than S-A.) The k- ω results for C_d on the finest grid differ from each other by 0.5%. There should be negligible influence of pressure drag at this angle of attack for a symmetric airfoil; thus discrepancies must be attributed to boundary layer and surface shear.

Solutions from Cobalt and RavenCFD on the 2nd finest grid for both C_d and C_f differ from the benchmark values by less than 0.1% for S-A, 0.2% for SST, 3.2% low for SARC (vs. S-A), and 3.4% high for k- ω (vs. S-A and SST). These comparisons primarily indicate that the k- ω and SARC turbulence model results are relatively close to the other models but highlight differing implementations for modeling the eddy viscosity.

Fig. 7 shows the local C_f predicted values for the NACA 0012 at $\alpha = 0^\circ$ from the flow solvers' various RANS turbulence models for the 2nd finest grid; Figs. 7(b) and 7(c) show a closer view, where the scale zooms to 10% chord length. Over nearly the entire upper surface, differences among the same turbulence models but different solver stay below 0.5% for S-A and SST and below 1.0% for k- ω . Among the turbulence models, differences between S-A and SST remain below 1.5%, below 3% between S-A and k- ω , and 2–6% between S-A and SARC. Differences are significantly larger inside the region of predicted transition from laminar to turbulent boundary layer. For the SST model in this region, the maximum difference between Cobalt and CFL3D is 15%; 35% between RavenCFD and CFL3D; and 44% between Cobalt and RavenCFD. For the k- ω model in this region, the maximum difference between Cobalt and RavenCFD is 19%. The S-A models compare well with each other, even in this region, with maximum differences not exceeding 1.0%. Thus, it may be generally concluded the turbulence models are implemented correctly in the various flow solvers for a non-zero pressure gradient; however, further evaluation and validation would be prudent in cases where flow information must be accurate within and around the transition region.

For code verification, Table 2 shows observed order of accuracy, and for solution verification it shows total estimated uncertainty due to numerical error for C_d and C_f for several turbulence models in Cobalt and RavenCFD. All turbulence model results are better than or comparable to those for the turbulent flat plate and show less 1st-order behavior, most likely because the leading-edge singularity and intersecting boundary conditions are absent in this application. Because there are no FUN3D and CFL3D observed order and uncertainty data for comparison, one cannot confidently declare verified turbulence models for this case; however, since their performance is comparable to that of Cobalt and RavenCFD for the flat plate, which in turn were comparable to the NASA benchmark solutions for the flat plate, verification or at least some degree of confidence may be inferred. All evaluated turbulence models for this case display significantly less numerical uncertainty ($\leq 0.5\%$) than the experiment's measurement uncertainty (2.5%) [17]. Such solution behavior further indicates that the turbulence models are implemented correctly for this case.

Table 3 summarizes the model validation activity by comparing the RANS results with the experimental data of Ladson [17]. The SST results, except for FUN3D (albeit for the 2nd finest mesh rather than for the finest), all predict within 0.1% of the experimental measurement, an excellent agreement. For all flow solvers

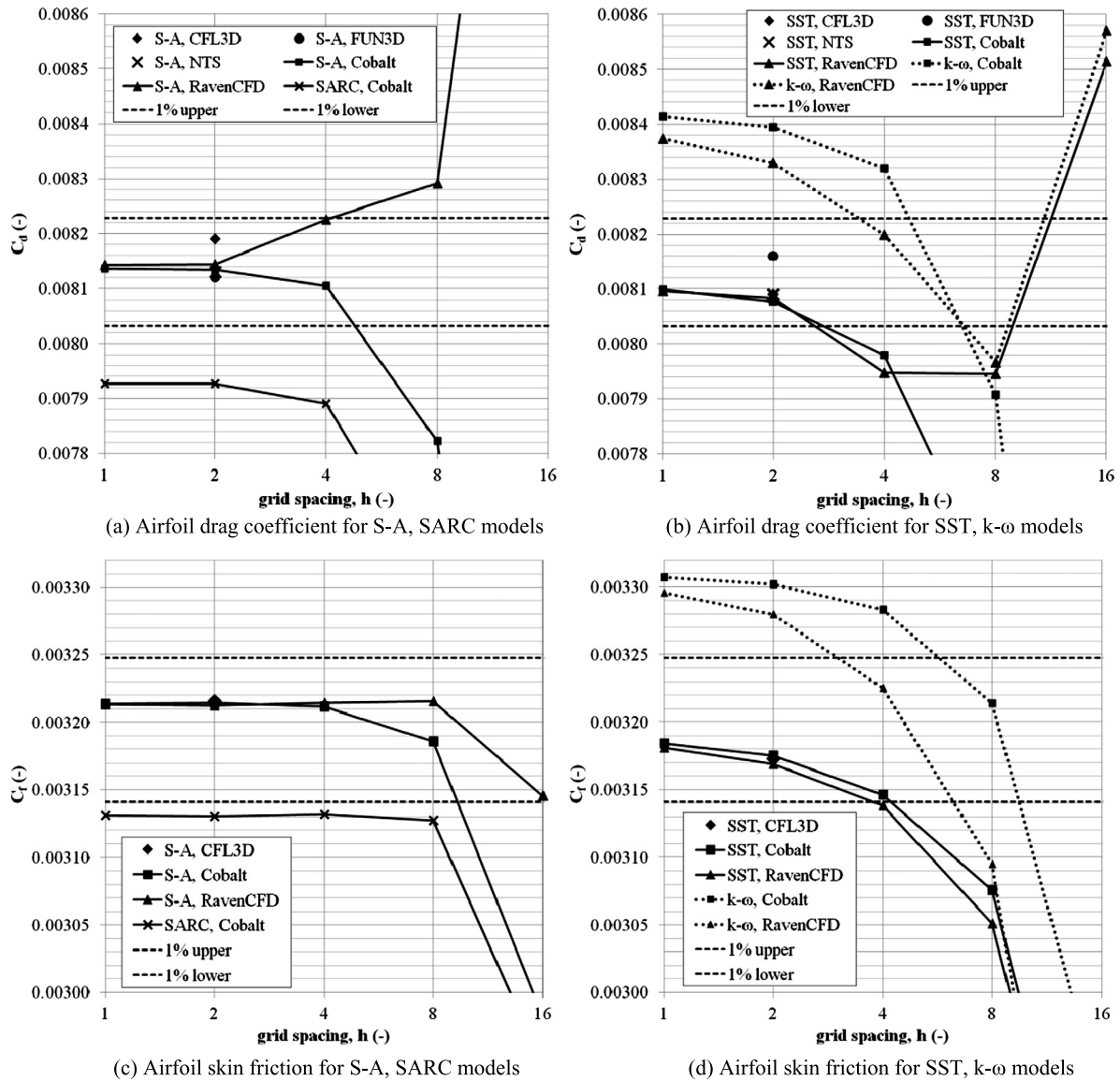


Fig. 6. NACA 0012, $\alpha = 0^\circ$, C_d and C_f from RANS turbulence models, $M_\infty = 0.15$, $Re_c = 6 \times 10^6$ ($c = 1$ m), $T_{ref} = 300$ K. Skin friction coefficient at $x/c = 0.51$, $y/c = 0.051$.

presented in the table, S-A, SST, and SARC predict C_d within the experimental uncertainty of 2.5%. Even the $k-\omega$ predictions match closely to experiment, differing by less than 4%. Thus, for the NACA 0012 airfoil at $\alpha = 0^\circ$, all the C_d predictions from the turbulence models under consideration match well with experiment. Additional comparisons of these four turbulence models show fair to good agreement with experiment for subsonic flow over various airfoils [6,11,12,30].

4. Summary and conclusions

The S-A turbulence model in NASA-Langley’s CFL3D and FUN3D flow solvers has been previously verified 2nd-order accurate [22], and for two unit-level applications this study has compared the NASA numerical benchmark solutions with solutions obtained from S-A, SARC, SST, and $k-\omega$ turbulence models in Cobalt and RavenCFD. Of the 36 total number of case evaluations (refer to Tables 1 and 2), the following seven cases clearly demonstrate solutions that approach 2nd-order observed accuracy ($1.8 \leq \hat{p} \leq 2.2$): for the flat plate, CFL3D S-A C_f , Cobalt SST C_f , Cobalt SARC C_f , and Cobalt $k-\omega$ C_d ; for the airfoil, Cobalt SST C_d , Cobalt $k-\omega$ C_d ,

and Cobalt $k-\omega$ C_f . This 2nd-order asymptotic behavior is not present in any other cases, despite the systematic mesh refinement. Considering that formal order of accuracy of the code may reduce to 1st order in the presence of the singularities noted, mixed-order solutions ($0.9 \leq \hat{p} \leq 2.2$) may be included; thus, 27 of the 36 evaluations, a clear majority, make the case for asymptotic behavior between 1st and 2nd order. Further, numerical uncertainty is estimated to be less than 1% in all of the 36 cases, less than 0.5% in 94% of the cases, and less than 0.1% in 61% of the cases. Thus, since Cobalt and RavenCFD turbulence models perform comparable to NASA’s verified models and since a majority of the case evaluations demonstrate reasonably asymptotic behavior, it is suggested that these turbulence models are implemented correctly (or are “pseudo-verified”) for these or similar flow conditions and configurations. Along with the pseudo-verification, this study identifies for these turbulence models where the largest errors exist and where to focus efforts to reduce the uncertainty, namely at and around singularities and coupled or conflicting boundary conditions. This study has also provided some turbulence model validation by comparing computational results with experiment. Specifically, this was accomplished by showing good

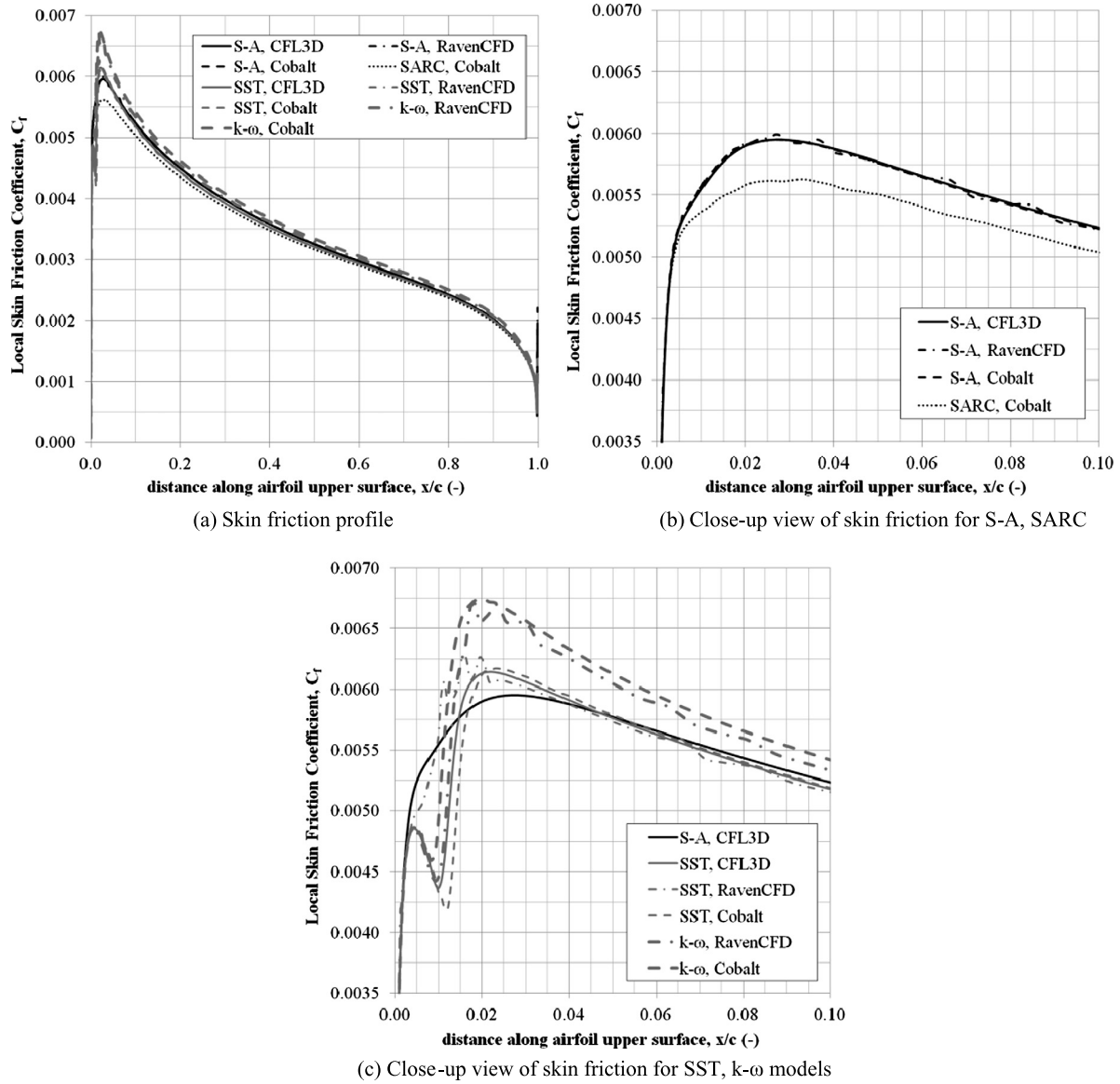


Fig. 7. C_f along NACA 0012 upper surface at $\alpha = 0^\circ$ from solutions on 2nd finest grid (897×257), $M_\infty = 0.15$, $Re_c = 6 \times 10^6$ ($c = 1$ m), $T_{ref} = 300$ K.

Table 2
NACA 0012 at $\alpha = 0^\circ$ observed order of accuracy and total numerical uncertainty.

NACA 0012 airfoil, $\alpha = 0^\circ$, $M = 0.15$, $Re_c = 6 \times 10^6$					
Turbulence model	Flow solver	C_d		C_f at $x/c = 0.51$, $y/c = 0.051$	
		\hat{p}	$U_{Tot, Num}$	\hat{p}	$U_{Tot, Num}$
S-A	Cobalt	3.55	0.03%	2.25	0.02%
	RavenCFD	5.78	0.02%	1.35	0.02%
SST	Cobalt	2.14	0.11%	1.70	0.28%
	RavenCFD	3.43	0.16%	1.33	0.02%
k- ω	Cobalt	1.94	0.10%	2.00	0.06%
	RavenCFD	1.59	0.52%	1.74	0.50%
SARC	Cobalt	6.84	0.004%	0.99	0.02%

agreement with experiment for the turbulent flat plate, where all the turbulence models show no more than 4.8% difference from experiment C_f values for $x/L > 0.05$, and where the models average between 1% (S-A, SST, SARC) and 2–3% difference from experiment. For the NACA 0012 case C_d at $\alpha = 0^\circ$, the S-A and SST models agree within 1.2% of experiment, the SARC model agrees within 2%, and k- ω within 4%.

Table 3
NACA 0012 at $\alpha = 0^\circ$ RANS turbulence models vs. experiment [17].

NACA 0012 airfoil, $\alpha = 0^\circ$, $M = 0.15$, $Re_c = 6 \times 10^6$				
Turbulence model	Flow solver	Grid	C_d	Diff (%)
Experiment, Ladson (1988)				
S-A	Cobalt	h_1	0.008137	0.55
		h_1	0.008143	0.63
	CFL3D	h_2	0.008190	1.21
	FUN3D	h_2	0.008120	0.35
	NTS	h_2	0.008130	0.47
SST	Cobalt	h_1	0.008099	0.09
		h_1	0.008096	0.05
	CFL3D	h_2	0.008090	-0.02
	FUN3D	h_2	0.008160	0.84
	NTS	h_2	0.008090	-0.02
k- ω	Cobalt	h_1	0.008414	3.98
	RavenCFD	h_1	0.008374	3.48
SARC	Cobalt	h_1	0.007927	-2.04

For future code verification studies, whether pure or comparative like this one, this study highlights the need for case models that are free of singularities and/or potentially coupled or conflict-

ing boundary conditions. Even so, the absence of singularities and intersecting boundary conditions does not guarantee clean verification, as noted in the airfoil case. An additional consideration is 2-D versus 3-D code verification. While flow velocities are low and geometries are simple in these cases, both turbulent flow and experimental measurement are fundamentally 3-D; thus, 2-D turbulence models may not accurately or correctly represent the actual flow physics, such that 3-D models should be considered for further verification and validation.

While the flow solvers, turbulence models, test cases, and these results are specific to this study, the *process* by which code and solution verification are conducted for commercial code may be broadly applied throughout the computational community.

Acknowledgements

The authors acknowledge the support of RavenCFD developer, James Carpenter of Corvid Technologies, and Cobalt developers, Robert Tomaro and William Strang of Cobalt Solutions. This work was supported in part by a grant of computer time from the Department of Defense (DoD) High Performance Computing Modernization Program at the US Army Engineer Research and Development Center, Vicksburg, Mississippi. The authors also acknowledge the work of Chris Rumsey, his colleagues at NASA-Langley, as well as partners in industry and academia, for their efforts to develop and maintain the collaborative website, “Turbulence Modeling Resource,” <http://turbmodels.larc.nasa.gov>.

References

- [1] F.S. Alvi, J.A. Ladd, W.W. Bower, Experimental and computational investigation of supersonic impinging jets, *AIAA J.* 40 (4) (2002) 599–609, <http://dx.doi.org/10.2514/2.1709>.
- [2] M.F. Barone, W.L. Oberkampf, F.G. Blottner, Validation case study: prediction of compressible turbulence mixing layer growth rate, *AIAA J.* 44 (7) (2006) 1488–1497, <http://dx.doi.org/10.2514/1.19919>.
- [3] I. Bassina, M. Strelets, P.R. Spalart, Response of simple turbulence models to step changes of slip velocity, *AIAA J.* 39 (2) (2001) 201–210, <http://dx.doi.org/10.2514/2.1301>.
- [4] E.D.V. Bigarella, J.L.F. Azevedo, Advanced eddy-viscosity and Reynolds-stress turbulence model simulations of aerospace applications, *AIAA J.* 45 (10) (2007) 2369–2390, <http://dx.doi.org/10.2514/1.29332>.
- [5] J.R. Carpenter, RavenCFD by Corvid Technologies, Flow Solver Documentation, <http://fileserv.corvidtec.com/dokuwiki/doku.php?id=ravencfd>, accessible with permission [cited 7 June 2012].
- [6] A. Celic, E.H. Hirschel, Comparison of eddy-viscosity turbulence models in flows with adverse pressure gradient, *AIAA J.* 44 (10) (2006) 2156–2169, <http://dx.doi.org/10.2514/1.14902>.
- [7] Cobalt version 5.0 user’s manual, Cobalt Solutions, LLC, Ohio, 2010.
- [8] Computational fluid dynamics, Corvid Technologies, <http://www.corvidtec.com/index.html>.
- [9] W.J. Devenport, J.A. Schetz, B. Vadapalli, Boundary layer codes for students in Java, version 2.1, Department of Aerospace and Ocean Engineering, Virginia Tech, Blacksburg, Virginia, <http://www.engapplets.vt.edu>.
- [10] J.R. Forsythe, W.Z. Strang, K.A. Hoffmann, Validation of several Reynolds-averaged turbulence models in a 3D unstructured grid code, *AIAA 2000-2552*, June 2000.
- [11] A. Garbaruk, M. Shur, M. Strelets, P.R. Spalart, Numerical study of wind-tunnel walls effects on transonic airfoil flow, *AIAA J.* 41 (6) (2003) 1046–1054, <http://dx.doi.org/10.2514/2.2071>.
- [12] M. Ghoreyshii, A. Jirasek, R.M. Cummings, Computational investigation into the use of response functions for aerodynamic-load modeling, *AIAA J.* 50 (6) (2012) 1314–1327, <http://dx.doi.org/10.2514/1.1J051428>.
- [13] J.J. Gottlieb, C.P.T. Groth, Assessment of Riemann solvers for unsteady one-dimensional inviscid flows of perfect gases, *J. Comput. Phys.* 78 (1988) 437–458, [http://dx.doi.org/10.1016/0021-9991\(88\)90059-9](http://dx.doi.org/10.1016/0021-9991(88)90059-9).
- [14] M.J. Grismer, W.Z. Strang, R.F. Tomaro, F.C. Witzeman, Cobalt: a parallel, implicit, unstructured Euler/Navier–Stokes solver, *Adv. Eng. Softw.* 29 (3–6) (1998) 365–373, [http://dx.doi.org/10.1016/S0965-9978\(97\)00075-6](http://dx.doi.org/10.1016/S0965-9978(97)00075-6).
- [15] K. Kitamura, E. Shima, Simple and parameter-free second slope limiter for unstructured grid aerodynamic simulations, *AIAA J.* 50 (6) (2012) 1415–1426, <http://dx.doi.org/10.2514/1.J051269>.
- [16] R.B. Kotapati-Apparao, K.D. Squires, J.R. Forsythe, Prediction of the flow over an airfoil at maximum lift, *AIAA 2004-0259*, January 2004.
- [17] C.L. Ladson, Effects of independent variation of Mach and Reynolds numbers on the low-speed aerodynamic characteristics of the NACA 0012 airfoil section, *NASA TM-4074*, October 1988.
- [18] W.L. Oberkampf, C.J. Roy, *Verification and Validation in Scientific Computing*, Cambridge University Press, Cambridge, England, 2010, Chaps. 2, 5, 7, 8, 10, 13.
- [19] C.J. Roy, W.L. Oberkampf, A comprehensive framework for verification, validation, and uncertainty quantification in scientific computing, *Comput. Methods Appl. Mech. Eng.* 200 (25–28) (2011) 2131–2144, <http://dx.doi.org/10.1016/j.cma.2011.03.016>.
- [20] C.L. Rumsey, Turbulence modeling resource, NASA-Langley Research Center, Hampton, Virginia, <http://turbmodels.larc.nasa.gov>.
- [21] C.L. Rumsey, P.R. Spalart, Turbulence model behavior in low Reynolds number regions of aerodynamic flowfields, *AIAA J.* 47 (4) (2009) 982–993, <http://dx.doi.org/10.2514/1.39947>.
- [22] C.L. Rumsey, J.L. Thomas, Application of FUN3D and CFL3D to the third workshop on CFD uncertainty analysis, *NASA TM-2008-215537*, November 2008.
- [23] J.A. Schetz, *Boundary Layer Analysis*, Prentice-Hall, New Jersey, 1993, Chaps. 2, 7.
- [24] M.L. Shur, M.K. Strelets, A.K. Travin, P.R. Spalart, Turbulence modeling in rotating and curved channels: assessing the Spalart–Shur correction, *AIAA J.* 38 (5) (2000) 784–792, <http://dx.doi.org/10.2514/2.1058>.
- [25] P.R. Spalart, M.L. Shur, On the sensitization of turbulence models to rotation and curvature, *Aerosp. Sci. Technol.* 1 (5) (1997) 297–302, [http://dx.doi.org/10.1016/S1270-9638\(97\)90051-1](http://dx.doi.org/10.1016/S1270-9638(97)90051-1).
- [26] E.F. Toro, M. Spruce, W. Speares, Restoration of the contact surface in the HLL-Riemann solver, *Shock Waves* 4 (1) (1994) 25–34, <http://dx.doi.org/10.1007/BF01414629>.
- [27] Unique contributions to the CFD discipline, Aerospace Engineering Computational Fluid Dynamics Laboratory, North Carolina State University, Raleigh, North Carolina, <http://www.mae.ncsu.edu/cfd/overview/intro.html> [cited 7 June 2012].
- [28] K. Wieghardt, W. Tillmann, On the turbulent friction layer for rising pressure, *NACA TM-1314*, October 1951.
- [29] K.E. Wurtzler, S.A. Morton, Accurate drag prediction using Cobalt, *AIAA 2004-0395*, January 2004.
- [30] J.-Y. Yang, T.-J. Hsieh, C.-H. Wang, Implicit weighted essentially nonoscillatory schemes with antidiffusive flux for compressible viscous flows, *AIAA J.* 47 (6) (2009) 1435–1444, <http://dx.doi.org/10.2514/1.38148>.